

## Deformation–wear transition map of DLC coating under cyclic impact loading

Mohd Fadzli Bin Abdollah<sup>a,\*</sup>, Yuto Yamaguchi<sup>a</sup>, Tsuyoshi Akao<sup>b</sup>, Naruhiko Inayoshi<sup>c</sup>,  
Nobuyuki Miyamoto<sup>c</sup>, Takayuki Tokoroyama<sup>a</sup>, Noritsugu Umehara<sup>a</sup>

<sup>a</sup> Department of Mechanical Science and Engineering, Graduate School of Engineering, Nagoya University, Furo-cho, Chikusa-ku, Nagoya 464-8603, Japan

<sup>b</sup> Technology Planning Department, DENSO Corporation, 1-1 Showa-cho, Kariya-shi, Aichi 448-8661, Japan

<sup>c</sup> Materials Engineering R&D Department, DENSO Corporation, 1-1 Showa-cho, Kariya-shi, Aichi 448-8661, Japan

### ARTICLE INFO

#### Article history:

Received 18 May 2011

Received in revised form

24 November 2011

Accepted 28 November 2011

Available online 6 December 2011

#### Keywords:

Impact testing

DLC coating

Deformation–wear transition map

Impact wear mechanisms

### ABSTRACT

A new deformation–wear transition map of hydrogen-free amorphous carbon coating (commonly known as Diamond-Like Carbon (DLC) coating) on tungsten high speed steel (SKH2) substrate under cyclic impact loading has been proposed to clarify the interactions of the operating parameters, deformation and wear. The study was carried out using an impact tester, under lubricated conditions over a wide range of impact cycles, and applied normal loads. SKH2 discs were coated with thin DLC films using a Physical Vapor Deposition (PVD) method. Tungsten (W) was used as an interlayer material. The DLC coated disc was impacted repeatedly by a chromium molybdenum steel (SCM420) pin. All impact tests were conducted at room temperature. It has been suggested that the deformation–wear transition map is an easy way to illustrate the impact wear mechanisms of DLC coating, as shown by its transition zones. Initially, the DLC coating only follows the plastic deformation of the substrate until several impact cycles. Then, a suppression of plastic deformation of the substrate is taking place due to the decreasing contact pressure with impact cycles to the yield point. Wear of the DLC coating becomes dominant when the critical limit of maximum normal impact load and impact cycles is exceeded. From experimental observations, some degradation of the DLC coating occurs within the wear zone.

© 2011 Elsevier B.V. All rights reserved.

### 1. Introduction

DLC has attracted great attention for many applications due to its tremendous properties, such as high hardness, thermal stability, low friction coefficient, and good chemical inertness. Furthermore, the DLC film showed an excellent wear resistance in dry and water- or oil-lubricated conditions [1]. The use of DLC coating, on the impact surfaces of components, provides high levels of protection against surface damage.

The concept of a ‘wear map’ was first discussed by Tabor [2], and was inspired by the pioneering work of Frost [3] on ‘deformation maps’. The development of deformation–wear transition map is a useful way to study and predict the transition of deformation to wear of one material impacting against another at different loads and cycles. Furthermore, the locations of the transition zones

within the operating parameters are important, in order to design engineer less component failures occurring prematurely.

Generally, the construction of transition maps follows two routes [4,5]. One is empirical: data from experiments are plotted on suitable axes and identified by wear rate or observation and boundaries are drawn to separate classes of behavior. The other route is that of physical modeling: model-based equations, describing the wear rate caused by each mechanism, are combined to give a map showing the total rate, and the field of dominance of each. However, only the empirical approach is used in this study.

The wear transition maps specific to certain materials, such as ceramics [6], grey cast iron [7], magnesium alloy [8], brass alloy [9], silicon nitride [10], have been developed extensively for a decade. All the transition maps, which appear in the above studies, were constructed using either a physical modeling or an empirical approach based on the sliding test data. However, in this century, there is still no development of deformation–wear transition map of the DLC coating under cyclic impact loading. Therefore, the aim of this study is to propose a new deformation–wear transition map of DLC coating based on variations of maximum normal impact loads and impact cycles. After a short description of the impact test used in this study, the construction of the deformation–wear transition map will be presented using experimental data and observations. The transition map of DLC coating, under cyclic impact loading,

\* Corresponding author. Tel.: +81 52 789 2788; fax: +81 52 789 2788.

E-mail addresses: [mohdfadzli@utem.edu.my](mailto:mohdfadzli@utem.edu.my) (M.F.B. Abdollah), [yamaguchi@ume.mech.nagoya-u.ac.jp](mailto:yamaguchi@ume.mech.nagoya-u.ac.jp) (Y. Yamaguchi), [TSUYOSHI.AKAO@denso.co.jp](mailto:TSUYOSHI.AKAO@denso.co.jp) (T. Akao), [NARUHIKO.INAYOSHI@denso.co.jp](mailto:NARUHIKO.INAYOSHI@denso.co.jp) (N. Inayoshi), [NOBUYUKI.MIYAMOTO@denso.co.jp](mailto:NOBUYUKI.MIYAMOTO@denso.co.jp) (N. Miyamoto), [tokoroyama@mech.nagoya-u.ac.jp](mailto:tokoroyama@mech.nagoya-u.ac.jp) (T. Tokoroyama), [ume@mech.nagoya-u.ac.jp](mailto:ume@mech.nagoya-u.ac.jp) (N. Umehara).

tends to focus on the description of its impact wear mechanisms and the transition between them.

## 2. Experimental method

### 2.1. Materials

The SKH2 disc was used as a substrate, whilst SCM420 pin was used as an impactor. The diameter of the disc and the pin were 10 mm and 2 mm, respectively (as shown in Fig. 1). All DLC films were deposited onto the SKH2 substrate using a PVD method; where W was used as an interlayer material. The film thickness  $h_c$  is approximately 2.97  $\mu\text{m}$ . The average surface roughness  $R_a$  of the as-deposited DLC coating is approximately 18.63 nm, which was measured by Atomic Force Microscopy (AFM). Material properties are listed in Table 1.

### 2.2. Impact testing

The impact test was performed using two self-developed impact testers, as shown in Fig. 2. The horizontal impact tester was used for more than  $10^2$  impact cycles, with a frequency of 10 Hz; and a drop-weight impact tester was used for the low impact cycles.

The impact test rig was designed to impact a DLC coated disc with a SCM420 pin for numerous impacts. Prior to the impact test, both disc and pin were cleaned using acetone in an ultrasonic bath. The DLC coated disc was repeatedly impacted at a  $90^\circ$  inclination at room temperature. Several different maximum normal impact loads were applied to the DLC coated disc via a spring system for the horizontal impact tester. Meanwhile, the maximum normal impact load of the drop-weight impact tester could be increased by adding an impactor mass  $m$ . It has been reported that the impactor mass does not significantly affect impact performances (deformation and wear) [11,12]. The applied load was observed by a load cell.

The surface morphology of the affected area on the DLC coating, as well as on the counterpart material, was observed by AFM, Field Emission Scanning Electron Microscopy (FE-SEM), and Energy Dispersive X-ray Spectroscopy (EDS). In addition, the Focused Ion

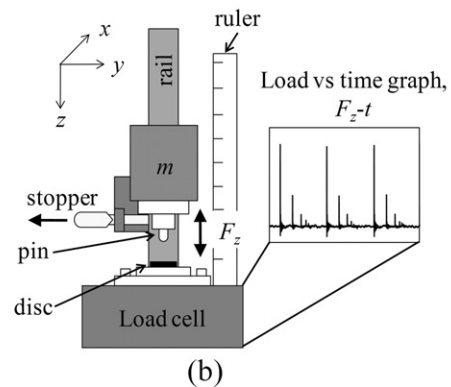
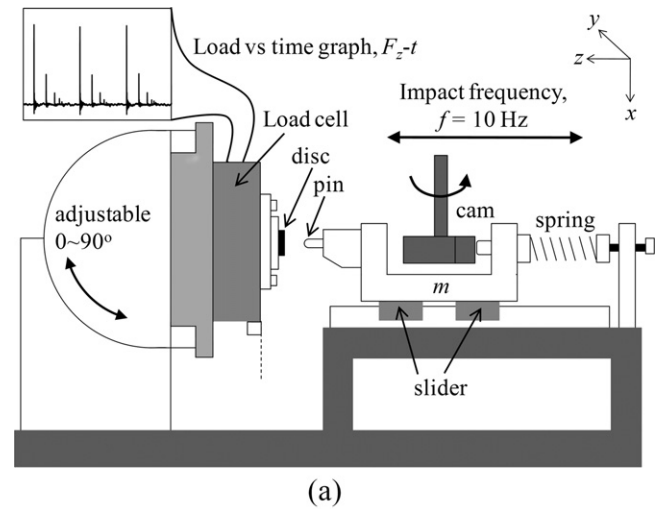


Fig. 2. Schematic illustration of the impact tester: (a) horizontal impact tester and (b) drop-weight impact tester.

Beam (FIB) was used to mill the tested sample, in order to examine the cross section of the DLC coating on the SKH2 substrate.

### 2.3. Residual impact crater volume/depth

The raw data collected included the measurements of the residual impact crater volume and its depth/radius. The depth  $h_r$  and radius  $a_r$  of the residual impact crater of the DLC coating were measured directly from a cross-sectional AFM topography image. The cross-sectional image, parallel to the  $y$ -axis, was taken at the center of impact crater, as shown in Fig. 3. In order to calculate the residual impact crater volume, raw data from the AFM was exported to OriginPro 8.1. An illustration of how the residual impact crater volume was calculated is shown in Fig. 3. The raw data of  $x$ -axis were discrete to  $n$  cross-sections with the thickness of  $\Delta x$ . The surface area  $A$  of each cross-section was determined using the integration method function in OriginPro 8.1. The residual impact crater volume  $V_r$  is determined using the following equation:

$$V_r = \sum_{j=1}^{n-1} (A \times \Delta x)_j \quad (1)$$

### 2.4. Transition of contact pressure

In this present paper, the loading conditions are beyond the elastic limit. Therefore, Hertz's contact calculation theory is not strictly applicable. However, Hertz's calculation was applied using the following assumption as one index of contact pressure [13]:

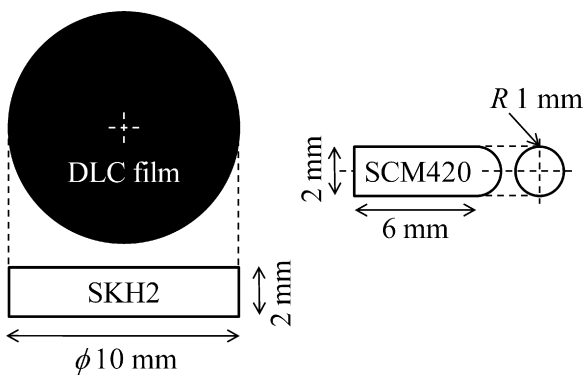


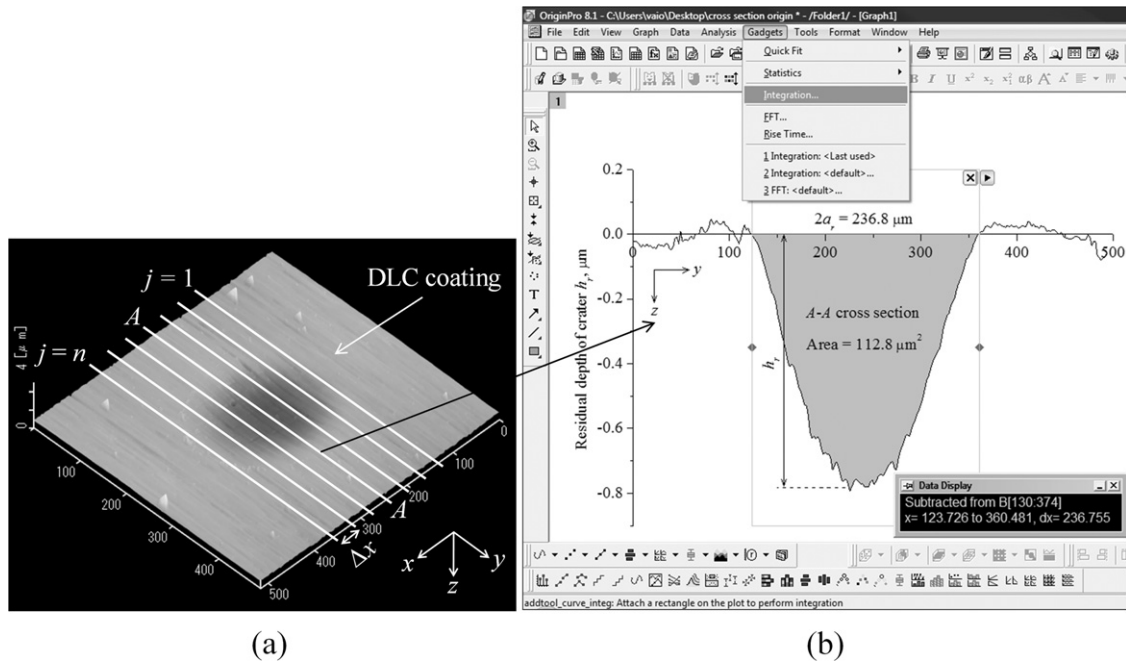
Fig. 1. Dimensions of the DLC coated disc and the SCM420 pin.

Table 1  
Material properties of the DLC, SKH2 substrate and SCM420 pin.

Properties	DLC	SKH2	SCM420
Young modulus, $E$ (GPa)	251	378	295
Poisson's ratio, $\nu$	0.3	0.3	0.3
Hardness, $H$ (GPa) <sup>a</sup>	17.14	9.80	7.43
Yield strength, $Y$ (GPa) <sup>b</sup>	6.12	3.50	2.65

<sup>a</sup> From the nanoindentation test.

<sup>b</sup>  $Y = H/2.8$ .



**Fig. 3.** (a) Discretions of  $x$ -axis of an impact crater to  $n$  cross sections, with the thickness of  $\Delta x$  and (b) determination of each surface area ( $A$ - $A$  cross section) using the integration function in OriginPro 8.1.

- (a) Contact condition is assumed to be point contact.
- (b) The major ( $y$ ) axis and minor ( $x$ ) axis of the residual contact radius, obtained experimentally from each impact cycle, is used.

Mean contact pressure  $p_{\text{mean}}$  for  $i$  impact cycles is calculated by using the following equation [14]:

$$p_{\text{mean},i} = \frac{F_z}{\pi(a_{rx}a_{ry})_i} \quad (2)$$

where  $F_z$  is the maximum normal impact load,  $a_{ry}$  and  $a_{rx}$  are the residual radii of the major and minor axes, respectively.

### 2.5. Wear measurements

In order to determine the wear depth of the DLC coating, its cross section on the SKH2 substrate was prepared using a FIB and observed by FE-SEM, as shown in Fig. 4. The tested sample was milled along the centre of the impact crater of the major axis. From Fig. 5, it is assumed that the wear depth  $h_w$  (measured from the FIB-milled cross-sectional image) is constant throughout the contact surface, and thus

$$h_p = h_r - h_w \quad (3)$$

where  $h_p$  is the plastic deformation depth and  $h_r$  is the residual depth of impact crater.

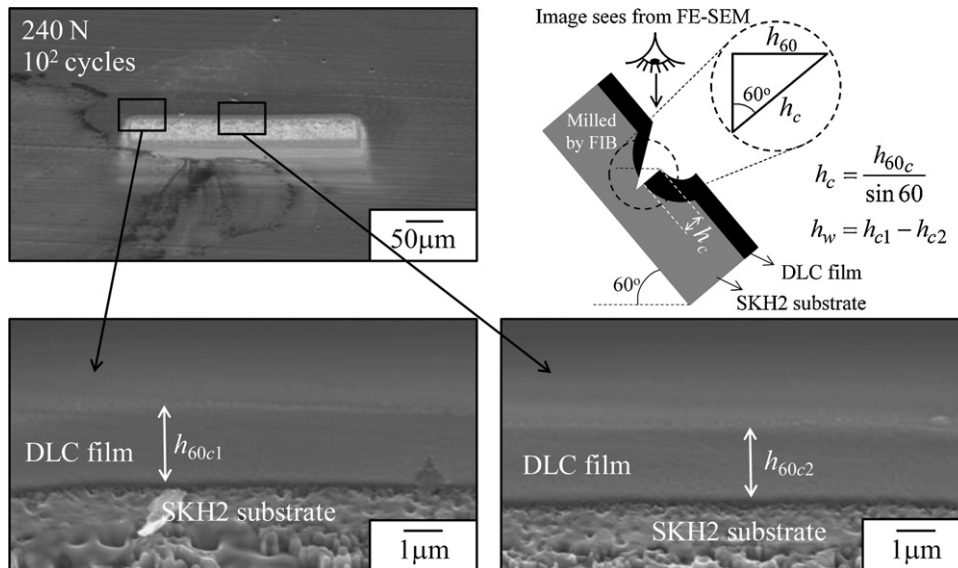


**Fig. 4.** FE-SEM cross-sectional view of the FIB-milled DLC coating on the SKH2 substrate (tilted at  $60^\circ$ ), where  $h_{60c1}$  is the non-impacted film thickness, and  $h_{60c2}$  is the impacted film thickness. The equations at the top right are for the wear depth  $h_w$  calculation.

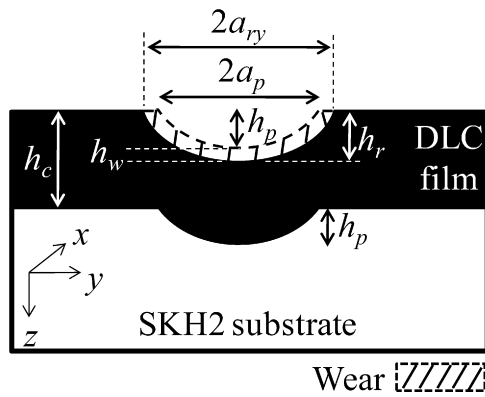


Fig. 5. Schematic illustration of the wear depth  $h_w$ .

### 2.6. Construction of the deformation–wear transition map

In this study, the construction of the deformation–wear transition map is a combination of procedures by Ashby and Lim [5] and Shu and Shen [6].

No universal deformation–wear transition map exists, because the controlling variables differ from mechanism to mechanism. Therefore, suitable axes of the map have to be decided. In this study, the appropriate axes are determined to be the maximum normal impact load  $F_z$  and the impact cycles  $N$ . These variables were chosen for two reasons: firstly, they directly determine the residual impact crater volume and secondly, they are under the control of the operator, and easily measured.

All data points of the residual impact crater volume  $V_r$  are plotted as functions of  $F_z$  and  $N$ , as shown in Fig. 6. Some interpolations and extrapolations are needed to obtain an evenly distributed data set. Then, the locations of both load- and impact cycle-dependent deformation–wear transitions, are identified by experimental observations and data trend analysis. Arrows indicate the onset of these variable-dependent deformation–wear transitions. The best fitting curves connecting all of the transition points are then traced and illustrated in the graph of  $F_z$  vs.  $N$ , as shown in Fig. 7. These curves represent the deformation–wear transition boundary of the impacted DLC coating.

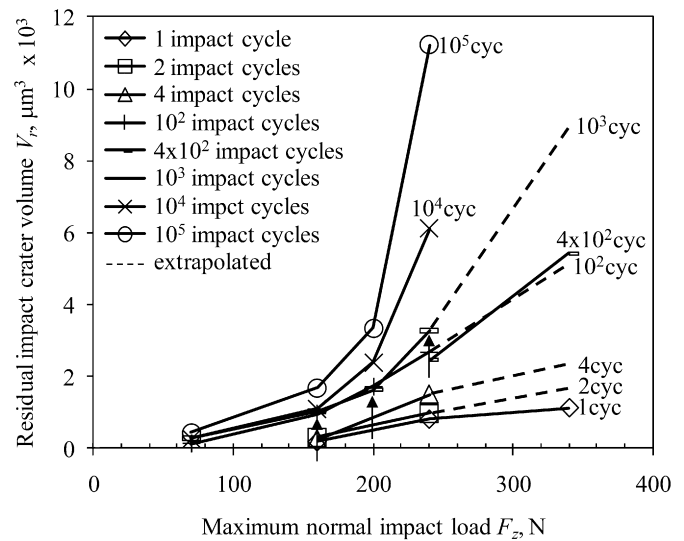
## 3. Results and discussion

### 3.1. Deformation–wear transition map

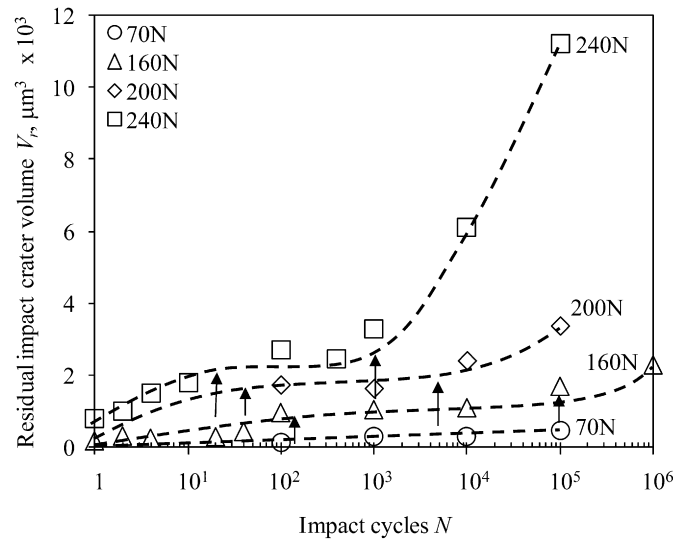
The maximum normal impact load and impact cycles are both important parameters and either variable can induce a transition from deformation to wear of DLC coating, as shown in Fig. 6. Therefore, a deformation–wear transition map was generated by simultaneously varying the maximum normal impact load and impact cycles, which revealed this transition very well.

Besides, the impact wear mechanisms of the DLC coating can easily be shown by its transition zones on the deformation–wear transition map, as shown in Fig. 7. Three zones were identified:

(a) The plastic deformation of the substrate zone, where the residual impact crater volume changes with the maximum normal impact load and impact cycles. As demonstrated in previous experiment [12], the deformation of an elastic–perfect plastic substrate should not be altered by the presence of a thin film, which itself simply follows the deformation of the substrate at the interface. The strain in the film is governed by the surface strain of the substrate. Furthermore, Fig. 8 clearly shows that almost no wear is observed at 70 and 160 N of the maximum normal impact load. In addition, the wear depth is almost zero



(a)



(b)

Fig. 6. Residual impact crater volume of the impacted DLC coating, plotted as a function of (a) maximum normal impact load and (b) impact cycles. (Arrows indicate the onset of load/cycle-dependent deformation–wear transitions.)

at 200 and 240 N under low impact cycles. This therefore reveals that only plastic deformation of the substrate has occurred.

(b) Suppression of plastic deformation of the substrate zone, where the residual impact crater volume remains constant with the impact cycles. This is due to the decreasing contact pressure with impact cycles to the yield point, as shown in Fig. 9. As the number of impact cycles is increased, the contact area spreads. Additionally, this experiment was under the constant maximum normal impact load for each impact cycle, and therefore, the contact pressure is decreased. In this zone, the deformation of substrate is most likely to undergo an elastic deformation if the contact pressure is almost or below its yield point. By increasing the maximum normal impact load, the suppression of plastic deformation of the substrate taking place, is faster. At 240 N of maximum normal impact load, the plastic deformation of the substrate is suppressed after  $10^1$  impact cycles, because the contact pressure starts to approach the yield point, as shown in Fig. 9. However, the plastic deformation of the substrate at 160 N starts to suppress after  $10^2$  impact cycles for the same

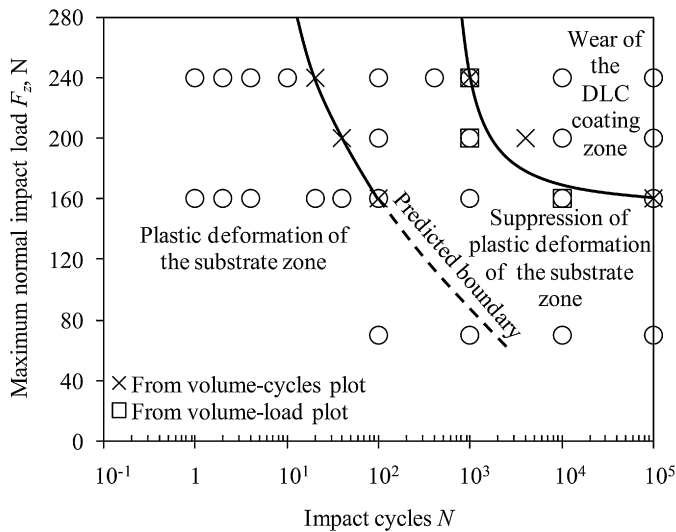


**Fig. 7.** Deformation-wear transition map of DLC coating under cyclic impact loading. The illustration of the predicted boundary is based on the contact pressure approaching the yield point.

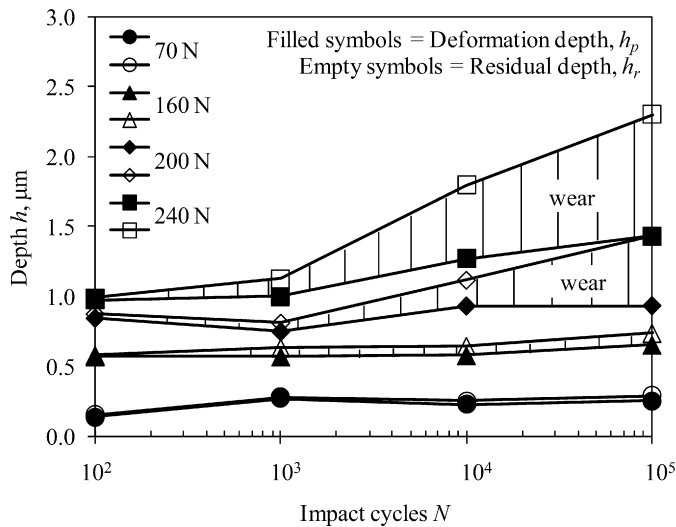


**Fig. 8.** Comparison of the residual depth of the impact crater  $h_r$  and the plastic deformation depth  $h_p$  as a function of the impact cycles. The difference between both curves (patterned in vertical lines) gives the approximate wear depth of the DLC coating.

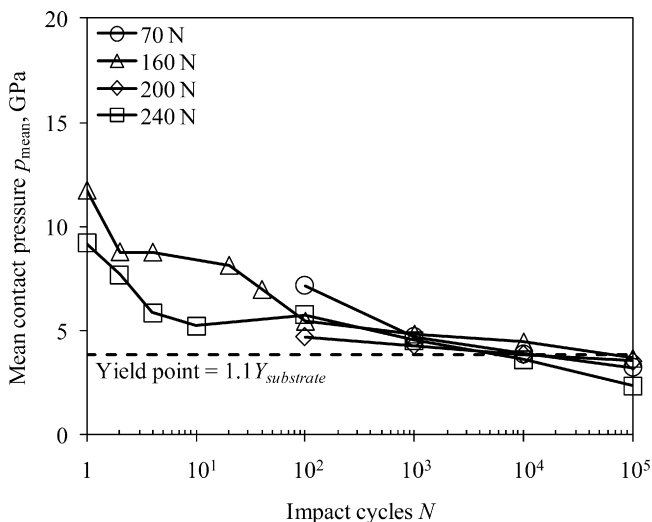


**Fig. 9.** Relationship between mean contact pressure and impact cycles.

reason. The predicted boundary, shown in Fig. 7, is illustrated based on the contact pressure approaching the yield point.

(c) Wear of the DLC coating zone, where the residual impact crater volume increases rapidly/radically with the maximum normal impact load and impact cycles. A critical maximum normal impact load and a critical impact cycle exists that will precipitate the wear transition of the DLC coating. Moreover, at those critical impact loads and impact cycles, wear gradually rises as material is worn away. Fig. 8 shows that no wear occurs if the maximum normal impact load is very small, but a wear transition occurs (due to the impact cycles) when the maximum normal impact load reaches above 160 N. Generally, the presence of a transfer layer on the counterpart material after repeated impacts modifies the tribological contact from that of SCM420/DLC to DLC/DLC; and a significant temperature may result at the contact point due to the low thermal conductivity of DLC, thus promoting graphitization. In addition, interface failures can be found, where the coating loses adhesion to the substrate due to both shear and tensile stress [15]. Cracks may start from defects at the interface and sometimes cause catastrophic failure with delamination of rather big flakes of the coating. If the load is high enough, cohesive failures and fatigue can also be found [15]. The cohesive failures normally consist of a continuous removal of the coating, starting from the middle of the spherical calotte. The fatigue occurs due to periodical stress loads and shows micro-cracks within the coating. Consequently, the increase in wear, as the maximum normal impact load and impact cycles is increased, may be due to the combination of graphitization and cracking from cyclic impact loading. This is in agreement with this study, where some degradation of the DLC coating, such as crack propagation of the film, phase transformation, and a tribochemical reaction of the wear debris/transfer layer, was observed. In addition, the formation of a transfer layer on the affected area of the counterpart material was also observed experimentally in this zone. Details about this wear will be briefly discussed in Section 3.2.

### 3.2. Degradation of DLC coating within the wear zone

#### 3.2.1. Crack propagation

As the thin hard coating fully transmits the impact generated stress field to the ductile substrate, the substrate undergoes a large

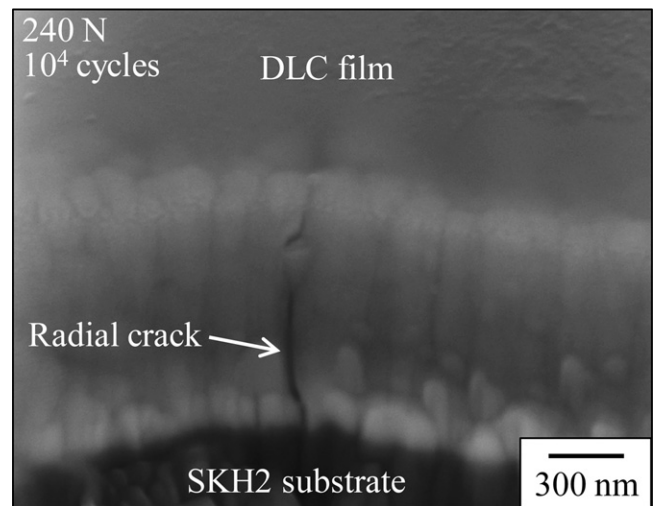


**Fig. 10.** The FE-SEM cross-sectional view of the FIB-milled DLC coating on the SKH2 substrate shows radial crack formation in the impacted area of the DLC film after  $10^4$  impact cycles at 240 N.

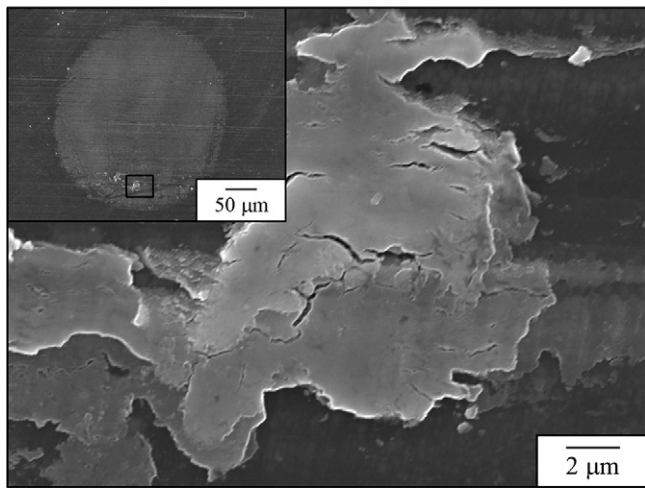


**Fig. 11.** FE-SEM micrograph of the wear debris taken from the edge of impact crater. The top-left micrograph is an impact crater.

plastic deformation (large indent depth) that the coating cannot accommodate other than by developing a network of cracks. Radial cracks can therefore be observed in the DLC film, as shown in Fig. 10. This micrograph has been taken after  $10^4$  impact cycles at 240 N, using FE-SEM. Radial cracking is observed in the coating below the impaction, which initiates from the coating/substrate interface and propagates upwards into the coating. The main reason for this is the low yield stress of the substrate, which allowed plastic strain under the impactor; which the hard and often brittle coating could not follow. To reduce the stress in the coating, it starts to build a radial crack inside the coating. The radial cracks observed in this study have also been identified in a study on indentation and scratching [16]. Tensile stress concentrations at

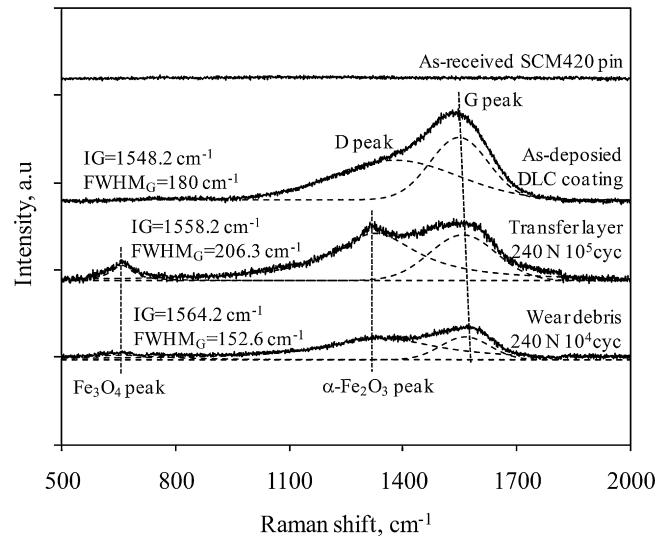


**Fig. 12.** Raman spectrum of the wear debris and transfer layer after  $10^4$  and  $10^5$  impact cycles at 240 N. The Raman spectrum of the as-received SCM420 pin and the as-deposited DLC coating are for comparison.

the coating/substrate interface during loading have been identified as a driving force that causes this type of crack [17,18].

### 3.2.2. Phase transformation and tribochemical reaction of wear debris and transfer layer

The wear debris of the impacted DLC coating were only observed on the edge of the impact craters, as shown in Fig. 11. In the case of a continuous presence of oil lubricant, the generated debris combined with oil, and removed progressively by its evacuation outside of the impact craters. However, some of the wear debris transferred to the counterpart material, as a transfer layer. The graphitization of wear debris, as well as the transfer layer, is confirmed by the

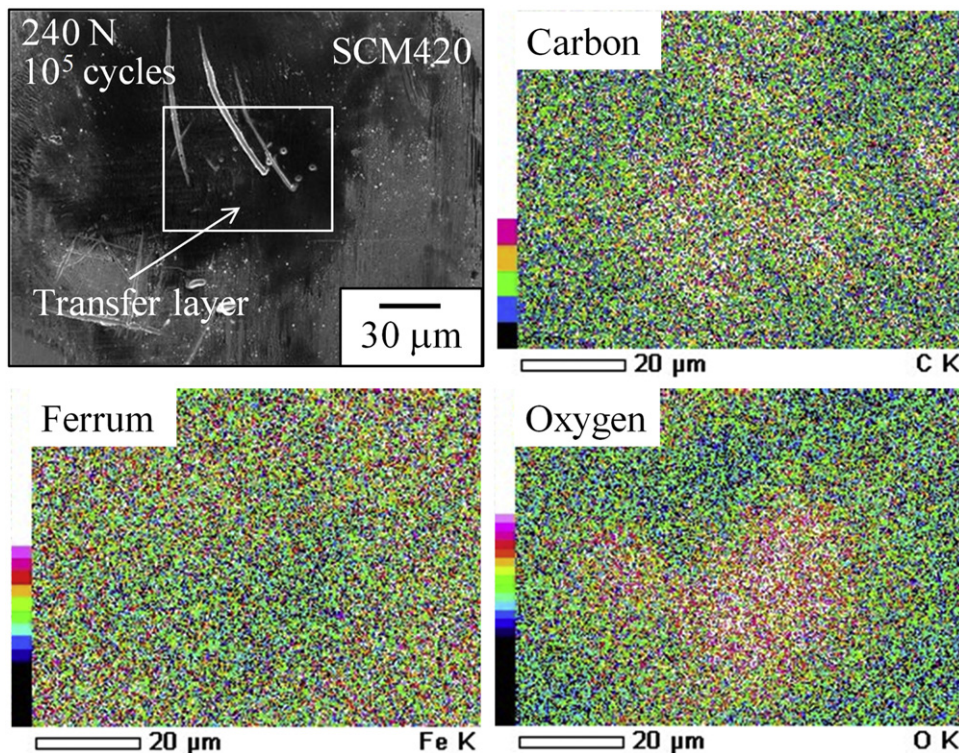


**Fig. 13.** The EDS maps (within a small rectangle in the FE-SEM micrograph) of the transfer layer on the affected area of the SCM420 pin.

Raman spectroscopy study [19]. From Fig. 12, the G peak of the wear debris shifted to a higher frequency compared to the as-deposited DLC coating. Therefore, this means that the  $sp^2$  bonding fraction increases, partial tetrahedral bonds have been broken, and have transformed into trigonal bonds [20]. The decrease in the  $FWHM_G$  indicated the removal of a bond angle disorder and the increasing dominance of crystallites [20]. From the analysis above, the  $sp^2$  coordinated carbon becomes gradually dominant and causes phase transformation from  $sp^3$  to  $sp^2$ , which would induce graphitization.

As for the transfer layer, the graphitization is expected to occur since it mainly comes from the wear debris. This is confirmed as the G peak is shifted to higher frequency than that of the as-deposited DLC coating, as shown in Fig. 12. However, the widening of its  $FWHM_G$ , after  $10^5$  impact cycles at 240 N, suggests that the size of the larger  $sp^2$  clusters is reduced due to the mechanical crush of the larger  $sp^2$  clusters.

In addition, the tribochemical reaction to the environment during impact occurred at the mating material where the transfer layer adhered; as well as in the wear debris [19]. This was due to the oxidation of ferrum (Fe) to magnetite ( $Fe_3O_4$ ) and hematite ( $\alpha-Fe_2O_3$ ) phases with a predominant peak at approximately  $680\text{ cm}^{-1}$  and  $1317\text{ cm}^{-1}$ . The broad peak at about  $1350\text{ cm}^{-1}$ , which is probably due to the disordered graphite (D peak), overlapped with the  $\alpha-Fe_2O_3$  peak. Thus, the D peak is not clearly visible in Fig. 12.

### 3.2.3. Formation of the transfer layer

Under tribological conditions, the softer of the two materials will usually be worn. In the case of DLC, this situation may be different since the wear of DLC, which has a graphitic nature, can be deposited onto the partner surface, forming the so-called transfer layer. The DLC then contacts against its own transfer layer and even though it is the harder surface, only the DLC is worn at a very low wear rate, whereas the softer partner surface will not be worn. The EDS maps (as shown in Fig. 13) confirm that the DLC coating transferred to the counterpart material of SCM420 pin after  $10^5$  impact cycles at 240 N.

## 4. Conclusions

A new deformation–wear transition map of DLC coating has been proposed using the test results to study of how individual impact parameters such as maximum normal impact load and impact cycles influence this transition.

The impact wear mechanisms of the DLC coating can easily be shown by its transition zones on the deformation–wear transition map. Three zones have been identified as follows:

- (a) The plastic deformation of the substrate zone: the residual impact crater volume increases with the maximum normal impact load and impact cycles. Only the substrate is plastically deformed. In addition, wear has not been observed in this zone.
- (b) Suppression of plastic deformation of the substrate zone: the residual impact crater volume remains constant with the impact cycles and plastic deformation of the substrate no longer appears. This is due to the decreasing contact pressure with impact cycles to the yield point.

- (c) Wear of the DLC coating zone: the residual impact crater volume increases rapidly/radically with the maximum normal impact load and impact cycles, due to material loss. The DLC coating appears to approach a high degree of wear when the critical limit of maximum normal impact load and impact cycles is exceeded. This wear is associated with some degradation of the DLC coating, such as the propagation of radial cracks in the DLC film, phase transformation of the wear debris/transfer layer, and its tribochemical reaction with the environment. In addition, formation of a transfer layer on the counterpart material has also been observed experimentally in this zone.

## Acknowledgments

The author Mohd Fadzli Bin Abdollah gratefully acknowledges the scholarship from Universiti Teknikal Malaysia Melaka (UTeM) for his Doctoral study.

## References

- [1] K. Holmberg, H. Ronkainen, A. Matthews, Tribology of thin coatings, *Ceram. Int.* 26 (2000) 787–795.
- [2] D. Tabor, Status and direction of tribology as a science in the 80s: understanding and prediction, in: *Proc. Int. Conf. Tribol.* 80s, vol. 1, 1984, pp. 1–17.
- [3] H.J. Frost, M.F. Ashby, *Deformation Mechanism Maps: The Plasticity and Creep of Metals and Ceramics*, first ed., Pergamon Press, Oxford, New York, 1982.
- [4] S.C. Lim, M.F. Ashby, Wear-mechanism maps, *Acta Metall.* 35 (1987) 1–24.
- [5] M.F. Ashby, S.C. Lim, Wear-mechanism maps, *Scripta Metall.* 24 (1990) 805–810.
- [6] S.M. Hsu, M.C. Shen, Ceramic wear maps, *Wear* 200 (1996) 154–175.
- [7] A.R. Riahi, A.T. Alpas, Wear map for grey cast iron, *Wear* 255 (2003) 401–409.
- [8] H. Chen, A.T. Alpas, Sliding wear map for the magnesium alloy Mg–9Al–0.9Zn (AZ91), *Wear* 246 (2000) 106–116.
- [9] K. Elleuch, R. Elleuch, R. Mnif, V. Fridrici, P. Kapsa, Sliding wear transition for the CW614 brass alloy, *Tribol. Int.* 39 (2006) 290–296.
- [10] J.R. Gomes, A.S. Miranda, J.M. Vieira, R.F. Silva, Sliding speed-temperature wear transition maps for  $Si_3N_4$ /iron alloy couples, *Wear* 250 (2001) 293–298.
- [11] P. Robinson, G.A.O. Davies, Impactor mass and specimen geometry effects in low velocity impact of laminated composites, *Int. J. Eng.* 12 (1992) 189–207.
- [12] M.F.B. Abdollah, Y. Yamaguchi, T. Akao, N. Inayoshi, T. Tokoroyama, N. Umehara, The effect of maximum normal impact load, absorbed energy, and contact impulse on the impact crater volume/depth of DLC coating, *Tribol. Online* 6 (2011) 257–264.
- [13] T. Yoshimi, S. Matsumoto, Y. Tozaki, T. Yoshida, H. Sonobe, T. Nishide, Work hardening and change in contact condition of rolling contact surface with plastic deformation, *Tribol. Online* 4 (2009) 1–5.
- [14] K.L. Johnson, *Contact Mechanics*, first ed., Cambridge University Press, Cambridge, 1985.
- [15] C.P.O. Treutler, Industrial use of plasma deposited coatings for components of automotive fuel injection systems, *Surf. Coat. Technol.* 200 (2005) 1969–1975.
- [16] Z.H. Xie, R. Singh, A. Bendavid, P.J. Martin, P.R. Munroe, M. Hoffman, Contact damage evolution in a diamond-like carbon (DLC) coating on a stainless steel substrate, *Thin Solid Films* 515 (2007) 3196–3201.
- [17] A.C. Fischer-Cripps, B.R. Lawn, A. Pajares, L. Wei, Stress analysis of elastic–plastic contact damage in ceramic coatings on metal substrates, *J. Am. Ceram. Soc.* 79 (1996) 2619–2625.
- [18] A. Abdul-Baqi, E. Van der Giessen, Numerical analysis of indentation-induced cracking of brittle coatings on ductile substrates, *Int. J. Solid Struct.* 39 (2002) 1427–1442.
- [19] M.F.B. Abdollah, Y. Yamaguchi, T. Akao, N. Inayoshi, N. Umehara, T. Tokoroyama, Phase transformation studies on the a-C coating under repetitive impacts, *Surf. Coat. Technol.* 205 (2010) 625–631.
- [20] J.T. Jiu, H. Wang, C.B. Cao, H.S. Zhu, The effect of annealing temperature on the structure of diamond-like carbon films by electrodeposition technique, *J. Mater. Sci.* 34 (1999) 5205–5209.